Petroleum Science 20 (2023) 2822–2834

Contents lists available at ScienceDirect

Petroleum Science

journal homepage: www.keaipublishing.com/en/journals/petroleum-science

Original Paper

A high resolution inversion method for fluid factor with dynamic dry-rock V_P/V_S ratio squared

Lin Zhou [a], Jian-Ping Liao [a], Xing-Ye Liu [b, *], Pu Wang [c], Ya-Nan Guo [d], Jing-Ye Li [e]

[a] School of Earth Sciences and Spatial Information Engineering, Hunan University of Science and Technology, Xiangtan 411201, Hunan, China
[b] Key Laboratory of Earth Exploration and Information Technology of Ministry of Education, College of Geophysics, Chengdu University of Technology, Chengdu 610059, Sichuan, China
[c] Hunan Key Laboratory of Nonferrous Resources and Geological Hazards Exploration, School of Geoscience and Info-Physics, Central South University, Changsha 410083, Hunan, China
[d] Exploration & Development Research Institute, PetroChina, Qinghai Oilfield Company, Dunhuang 736202, Gansu, China
[e] College of Geophysics, China University of Petroleum (Beijing), Beijing 102249, China

ARTICLE INFO

Article history:
Received 7 November 2022
Received in revised form
11 July 2023
Accepted 14 September 2023
Available online 16 September 2023

Edited by Jie Hao and Meng-Jiao Zhou

Keywords:
Fluid factor
Dry-rock V_P/V_S ratio squared (DVRS)
Dynamic variable
Multiple parameters simultaneous inversion
Generalized nonlinear inversion (GNI)

ABSTRACT

As an important indicator parameter of fluid identification, fluid factor has always been a concern for scholars. However, when predicting Russell fluid factor or effective pore-fluid bulk modulus, it is necessary to introduce a new rock skeleton parameter which is the dry-rock V_P/V_S ratio squared (DVRS). In the process of fluid factor calculation or inversion, the existing methods take this parameter as a static constant, which has been estimated in advance, and then apply it to the fluid factor calculation and inversion. The fluid identification analysis based on a portion of the Marmousi 2 model and numerical forward modeling test show that, taking the DVRS as a static constant will limit the identification ability of fluid factor and reduce the inversion accuracy. To solve the above problems, we proposed a new method to regard the DVRS as a dynamic variable varying with depth and lithology for the first time, then apply it to fluid factor calculation and inversion. Firstly, the exact Zoeppritz equations are rewritten into a new form containing the fluid factor and DVRS of upper and lower layers. Next, the new equations are applied to the four parameters simultaneous inversion based on the generalized nonlinear inversion (GNI) method. The testing results on a portion of the Marmousi 2 model and field data show that dynamic DVRS can significantly improve the fluid factor identification ability, effectively suppress illusion. Both synthetic and filed data tests also demonstrate that the GNI method based on Bayesian deterministic inversion (BDI) theory can successfully solve the above four parameter simultaneous inversion problem, and taking the dynamic DVRS as a target inversion parameter can effectively improve the inversion accuracy of fluid factor. All these results completely verified the feasibility and effectiveness of the proposed method.

1. Introduction

How to effectively identify reservoir fluid has always been the focus of reservoir exploration. A large number of geophysicists have carried out relevant researches to improve the quality of fluid discrimination (Wang et al., 2020, 2021). Smith and Gidlow (1987) put forward the concept of fluid factor for the first time, and demonstrated the advantages of fluid factor in fluid identification through practical application. After that, the fluid factor has received a lot of attention and development. Goodway et al. (1997), Gray et al. (1999), Russell et al. (2003, 2011), Du and Yan (2013), Yin and Zhang (2014) and Li (2014) have defined different fluid factor forms from different perspectives. For example, the product of density and shear modulus ($\rho\mu$), the product of compression modulus and density ($\lambda\rho$), Russell fluid factor f ($f = \rho V_P^2 - \gamma_{dry}^2 \rho V_S^2$, $\gamma_{dry}^2 = (V_P/V_S)_{dry}^2$ is the dry-rock V_P/V_S ratio squared (DVRS)), the product of Russell fluid factor and density (ρf), $F_\rho = (\rho V_P)^2 - ((3V_P^2 - 4V_S^2)/(V_P^2 - V_S^2))(\rho V_S)^2$ and the effective pore-fluid bulk modulus (K_f). In fact, except Russell fluid factor f and

* Corresponding author.
E-mail address: lxylxx@cdut.edu.cn (X.-Y. Liu).

https://doi.org/10.1016/j.petsci.2023.09.015

effective pore-fluid bulk modulus K_f derived from the poroelasticity theory, other forms of fluid factors have no clear physical meaning and the fluid identification ability is not representative. Therefore, f and K_f with clear physical meaning and good fluid identification performance are still the main target inversion parameters. Zong et al. (2013) proposed a direct inversion method for fluid factor f based on the Russell linear approximate formula. Chen et al. (2018) rewrote the three-term Russell linear approximate formula into two terms and developed a direct inversion method for fluid factor f, which improved the stability of inversion results. To improve the quality of fluid identification, Yin and Zhang (2014) defined the effective pore-fluid bulk modulus K_f as the fluid factor, and then derived a new linear approximate formula containing this fluid factor. Based on this linear approximate formula, they successfully estimated K_f using the Bayesian prestack inversion method. On the basis of Yin and Zhang's research, Du et al. (2019) further developed a matrix-fluid decoupling-based joint PP-PS-wave seismic inversion method, which effectively improving the estimation accuracy of fluid factor K_f. Zhou et al. (2021a) focused on the direct inversion method for fluid factor f based on the exact Zoeppritz equations, which overcomes the limitations of approximate formulas on the inversion accuracy of fluid factor f, and significantly improve the inversion accuracy and resolution. However, by analyzing the above researches, it can be found that these prestack inversion methods for fluid factors f and K_f take the DVRS as a static constant. Zhou et al. (2021a) pointed out that the static constant DVRS has a negative impact on the estimation accuracy of the fluid factor. In physical sense, the DVRS should varies with the different lithology at different depth (or travel time). If we take it as a static constant, and apply to the calculation of fluid factor f and the prestack inversion, it will inevitably degrade the identification ability of fluid factor f and the estimation accuracy of f and K_f. Hence, it is necessary to propose a new method to eliminate the influence of the static constant DVRS. In this paper, we will choose the Russell fluid factor f as the target inversion parameter to study how to solve this problem, so as to further improve the identification quality and estimation accuracy.

Once the DVRS is taken as the target inversion parameter at the same time, which means that the total target inversion parameters of the inversion algorithm increases from three to four. For the prestack AVO/AVA multi parameters nonlinear inversion problems constructed by nonlinear forward equations, the common solving methods are the fully nonlinear algorithm based on intelligent optimization algorithms and the generalized nonlinear algorithm (Bing et al., 2012; Zhe and Gu, 2013; Lu et al., 2018; Huang et al., 2020; Ali et al., 2020; Ashraf et al., 2020, 2021; Liu et al., 2020, 2022a, 2022b; Zhou et al., 2021a; 2021b, 2022). It is well known that the fully nonlinear algorithm is computationally expensive and difficult to be applied to huge field data inversion. Therefore, the generalized nonlinear algorithm based on Taylor series expansion has been widely used in solving such complex nonlinear inversion problems. Lu et al. (2015) successfully used the Levenberg-Marquardt (LM) method (Levenberg, 1944; Marquardt, 1963) to solve the nonlinear inversion problem constructed by the exact Zoeppritz equations. Similarly, Zhi et al. (2016) successfully solved the nonlinear inversion problem constructed by the exact Zoeppritz equations using the iteratively regularizing Levenberg-Marquardt (IRLM) method (Nocedal and Wright, 2006). Lu et al. (2018) combined the LM method with Gauss-Newton method to solve the nonlinear inversion problem of VTI media based on the exact Zoeppritz equations. Zhou et al. (2021a) developed a nonlinear inversion method based on the exact Zoeppritz equations using the Bayesian deterministic inversion (BDI) method, which further improved the estimation accuracy of reservoir parameters by introducing a prior information. Zhou et al. (2020, 2022) successfully solved the nonlinear simultaneous inversion problem of five parameters of VTI media using the BDI method. It can be seen that the LM method and the BDI method are the two most commonly used generalized nonlinear inversion (GNI) methods to solve multi parameters nonlinear inversion problems. In general, when the parameterized form of nonlinear equations changes, the stability of a GNI algorithm based on these equations will also changes. This means that it is unclear whether the LM method or BDI method can successfully solve the four parameters simultaneous nonlinear inversion problem based on the new parameterized exact Zoeppritz equations. In fact, the LM methods based on damped least squares algorithm and the BDI methods based Bayesian theory, both of them have their own advantages and disadvantages. The LM method might achieve stable inversion without introducing well constraint, which can solve the problem that it is difficult to accurately estimate the logging curve of the DVRS. The BDI method can further reduce the multiplicity of inversion and improve the stability and accuracy of inversion results by introducing a prior information contained in well data. In this paper, we first analyze and compare whether the IRLM method and the BDI method can successfully solve the four parameters simultaneous inversion problem of the Russell fluid factor (f), shear modulus (μ), density (ρ), and DVRS (γ^2_{dry}). Then, a more appropriate method is selected.

To reduce the negative influences of DVRS on the identification ability and inversion accuracy of fluid factor, it is studied for the first time as a dynamic variable varying with lithology and depth (or travel time), and takes it as another target inversion parameter. First, we derive the new exact Zoeppritz equations containing four unknown parameters, namely, the fluid factor, shear modulus, density and DVRS by further rewriting the new form of exact Zoeppritz equations containing fluid factor given by Zhou et al. (2021a). Then, the nonlinear inversion objective function is constructed using the new equations. Finally, the GNI method is selected according to the comparative analysis results to solve the corresponding nonlinear inversion objective function. Both synthetic and field data tests show that the proposed method can effectively overcome the adverse influence of the static constant DVRS, and improve the identification ability and the estimate accuracy of fluid factor.

2. Methodology

Forward equations are the core of inversion algorithms. Their parameterized form determines what parameters inversion results can be output, and their calculation accuracy determines the accuracy of parameter inversion results. Generally, the higher the calculation accuracy of forward equations, the higher the accuracy of inversion results. Therefore, to study the impact of static DVRS on the inversion results, we first analyze the influence of static DVRS on the calculation accuracy of forward equations. The traditional expressions of the exact Zoeppritz equations are nonlinear equations about the P- and S-wave velocities and density. Therefore, we first need to derive them into a form that includes the fluid factor and static constant DVRS using rock physics relations. Since the detailed derivation process was provided by Zhou et al. (2021a), we have not repeated in this paper. In addition, the design of interface models is also crucial when analyzing the calculation accuracy of forward equations. To make our analysis results more representative, we design four kinds of common stratigraphic interface models, namely, the shale and water sand interface model, the water-sand and gas sand interface model, the water sand and water sand interface model, and the shale and gas sand interface model.

2.1. The new form of the exact Zoeppritz equations

Zhou et al. (2021a) derived the new form of the Zoeppritz equations in terms of fluid factor, shear modulus, density and static DVRS (FMR-Zoeppritz equations), and their expressions are shown below:

$$\begin{bmatrix} -\sin\theta_1 & -\sqrt{1-\frac{\mu_1}{f_1+\gamma_{dry}^2\mu_1}\sin^2\theta_1} & \sqrt{\frac{\rho_1\left(f_2+\gamma_{dry}^2\mu_2\right)}{\rho_2\left(f_1+\gamma_{dry}^2\mu_1\right)}}\sin\theta_1 & \sqrt{1-\frac{\rho_1\mu_2}{\rho_2\left(f_1+\gamma_{dry}^2\mu_1\right)}\sin^2\theta_1} \\ \cos\theta_1 & -\sqrt{\frac{\mu_1}{f_1+\gamma_{dry}^2\mu_1}}\sin\theta_1 & \sqrt{1-\frac{\rho_1\left(f_2+\gamma_{dry}^2\mu_2\right)}{\rho_2\left(f_1+\gamma_{dry}^2\mu_1\right)}\sin^2\theta_1} & -\sqrt{\frac{\rho_1\mu_2}{\rho_2\left(f_1+\gamma_{dry}^2\mu_1\right)}}\sin\theta_1 \\ \sin 2\theta_1 & \sqrt{\frac{f_1+\gamma_{dry}^2\mu_1}{\mu_1}}-2\sqrt{\frac{\mu_1}{f_1+\gamma_{dry}^2\mu_1}}\sin^2\theta_1 & 2\frac{\mu_2}{\mu_1}\sqrt{\sin^2\theta_1-\frac{\rho_1\left(f_2+\gamma_{dry}^2\mu_2\right)}{\rho_2\left(f_1+\gamma_{dry}^2\mu_1\right)}\sin^4\theta_1} & \frac{\sqrt{\mu_2\left(f_1+\gamma_{dry}^2\mu_1\right)}}{\mu_1}\left(\sqrt{\frac{\rho_2}{\rho_1}}-2\frac{\mu_2\sqrt{\rho_1}}{\left(f_1+\gamma_{dry}^2\mu_1\right)\sqrt{\rho_2}}\sin^2\theta_1\right) \\ 2\frac{\mu_1}{f_1+\gamma_{dry}^2\mu_1}\sin^2\theta_1-1 & 2\frac{\mu_1\sin\theta_1}{f_1+\gamma_{dry}^2\mu_1}\sqrt{1-\frac{\mu_1}{f_1+\gamma_{dry}^2\mu_1}\sin^2\theta_1} & \sqrt{\frac{f_2+\gamma_{dry}^2\mu_2}{f_1+\gamma_{dry}^2\mu_1}}\left(\sqrt{\frac{\rho_2}{\rho_1}}-2\frac{\mu_2\sqrt{\rho_1}}{\left(f_1+\gamma_{dry}^2\mu_1\right)\sqrt{\rho_2}}\sin^2\theta_1\right) & -2\frac{\mu_2}{f_1+\gamma_{dry}^2\mu_1}\sqrt{\sin^2\theta_1-\frac{\rho_1\mu_2}{\rho_2\left(f_1+\gamma_{dry}^2\mu_1\right)}\sin^4\theta_1} \end{bmatrix}\begin{bmatrix} R_{PP} \\ R_{PS} \\ T_{PP} \\ T_{PS} \end{bmatrix}=\begin{bmatrix} \sin\theta_1 \\ \cos\theta_1 \\ \sin 2\theta_1 \\ 1-2\frac{\mu_1}{f_1+\gamma_{dry}^2\mu_1}\sin^2\theta_1 \end{bmatrix}. \quad (1)$$

where, f_1, f_2, μ_1, μ_2, ρ_1 and ρ_2 respectively represent the fluid factor, shear modulus and density at the upper and lower layers of the reflecting interface, θ_1 represents the incident angle of P-wave, and γ_{dry}^2 represents the DVRS. In these equations, γ_{dry}^2 is a known static constant, which needs to be determined before the inversion.

The parameters of four models we mentioned above are shown in Table 1. Here, the four models are used to analyze the impact of static constant γ_{dry}^2 on the calculation accuracy of the FMR-Zoeppritz equations. The analysis results are shown in Fig. 1.

From Fig. 1, it can be seen that setting the DVRS as a static constant will introduce significant computational errors. The negative influence of the introduced calculation errors on the inversion results cannot be ignored. Therefore, it is necessary to transform the γ_{dry}^2 in Eq. (1) into a dynamic variable. In this way, the FMR-Zoeppritz equations shown in Eq. (1) can be converted to the FMR-γ_{dry}^2-Zoeppritz equations shown in Eq. (2):

$$\begin{bmatrix} -\sin\theta_1 & -\sqrt{1-\frac{\mu_1}{f_1+\gamma_{dry1}^2\mu_1}\sin^2\theta_1} & \sqrt{\frac{\rho_1\left(f_2+\gamma_{dry2}^2\mu_2\right)}{\rho_2\left(f_1+\gamma_{dry1}^2\mu_1\right)}}\sin\theta_1 & \sqrt{1-\frac{\rho_1\mu_2}{\rho_2\left(f_1+\gamma_{dry1}^2\mu_1\right)}\sin^2\theta_1} \\ \cos\theta_1 & -\sqrt{\frac{\mu_1}{f_1+\gamma_{dry1}^2\mu_1}}\sin\theta_1 & \sqrt{1-\frac{\rho_1\left(f_2+\gamma_{dry2}^2\mu_2\right)}{\rho_2\left(f_1+\gamma_{dry2}^2\mu_1\right)}\sin^2\theta_1} & -\sqrt{\frac{\rho_1\mu_2}{\rho_2\left(f_1+\gamma_{dry1}^2\mu_1\right)}}\sin\theta_1 \\ \sin 2\theta_1 & \sqrt{\frac{f_1+\gamma_{dry1}^2\mu_1}{\mu_1}}-2\sqrt{\frac{\mu_1}{f_1+\gamma_{dry1}^2\mu_1}}\sin^2\theta_1 & 2\frac{\mu_2}{\mu_1}\sqrt{\sin^2\theta_1-\frac{\rho_1\left(f_2+\gamma_{dry2}^2\mu_2\right)}{\rho_2\left(f_1+\gamma_{dry2}^2\mu_1\right)}\sin^4\theta_1} & \frac{\sqrt{\mu_2\left(f_1+\gamma_{dry1}^2\mu_1\right)}}{\mu_1}\left(\sqrt{\frac{\rho_2}{\rho_1}}-2\frac{\mu_2\sqrt{\rho_1}}{\left(f_1+\gamma_{dry1}^2\mu_1\right)\sqrt{\rho_2}}\sin^2\theta_1\right) \\ 2\frac{\mu_1}{f_1+\gamma_{dry1}^2\mu_1}\sin^2\theta_1-1 & 2\frac{\mu_1\sin\theta_1}{f_1+\gamma_{dry1}^2\mu_1}\sqrt{1-\frac{\mu_1}{f_1+\gamma_{dry1}^2\mu_1}\sin^2\theta_1} & \sqrt{\frac{f_2+\gamma_{dry2}^2\mu_2}{f_1+\gamma_{dry1}^2\mu_1}}\left(\sqrt{\frac{\rho_2}{\rho_1}}-2\frac{\mu_2\sqrt{\rho_1}}{\left(f_1+\gamma_{dry1}^2\mu_1\right)\sqrt{\rho_2}}\sin^2\theta_1\right) & -2\frac{\mu_2}{f_1+\gamma_{dry1}^2\mu_1}\sqrt{\sin^2\theta_1-\frac{\rho_1\mu_2}{\rho_2\left(f_1+\gamma_{dry1}^2\mu_1\right)}\sin^4\theta_1} \end{bmatrix}\begin{bmatrix} R_{PP} \\ R_{PS} \\ T_{PP} \\ T_{PS} \end{bmatrix}=\begin{bmatrix} \sin\theta_1 \\ \cos\theta_1 \\ \sin 2\theta_1 \\ 1-2\frac{\mu_1}{f_1+\gamma_{dry1}^2\mu_1}\sin^2\theta_1 \end{bmatrix}. \quad (2)$$

where γ_{dry1}^2 and γ_{dry2}^2 respectively represent the DVRS at the upper and lower layers on both sides of reflecting interface.

In fact, setting the DVRS as a static constant not only reduces the calculation accuracy of reflection coefficients, but also limits the ability of fluid factor on formation fluid identification. Here, an extracted portion of the Marmousi 2 model (Martin et al., 2006) shown in Fig. 2 (the blue rectangular box indicates the area) is utilized to analyze the influence of DVRS on the fluid discrimination performance of Russell fluid factor f. According to the estimation method for the static DVRS proposed by Chen et al. (2018), the static DVRS value of the selected area is about 3.95. We can obtain the fluid factor profile that is shown in Fig. 3 by substituting this value into the fluid factor calculation formula. As Chen et al. (2018) described in their paper, the fluid factor based on the static DVRS estimated by their method can effectively distinguish water wet sand, oil charged sand and gas charged sand. However, we can also notice that when a same static DVRS value is used for the whole profile, water wet sand and dry sand cannot be effectively distinguished, which leads to the false interpretation and easy to identify the dry sand as water wet sand. To solve this problem, we will consider the impact of lithology and depth on the DVRS. Based on the density profile, we divide the selected profile into four regions along the vertical direction using three dotted lines shown in Fig. 4, and then estimate the DVRS value in these four regions respectively. Finally, a group of dynamic DVRS values are obtained, which are 5.44, 4.25, 3.68, and 3.67 respectively. Substituting these dynamic DVRS values into the fluid factor calculation formula, finally, the fluid factor profile shown in Fig. 5 is obtained. We find that the fluid factor profile calculated by dynamic DVRS values can not only effectively distinguish water wet sand, oil charged sand and gas charged sand, but also effectively distinguish water wet sand and dry sandstone. The above analysis shows that it is necessary to consider the DVRS as a dynamic parameter varying with lithology and depth when applying the Russell fluid factor to identify

Table 1
Parameters of four models.

Classify	Lithology	f, GPa	μ, GPa	ρ, g/cm^3	V_P, m/s	V_S, m/s	γ^2_{dry}
Model 1	Shale	7.279	5.509	2.40	3095	1515	2.852
	Water sand	4.678	13.983	2.32	4115	2455	2.475
Model 2	Gas sand	3.303	5.766	2.08	2780	1665	2.215
	Water sand	6.584	5.673	2.23	3050	1595	2.496
Model 3	Water sand	5.610	1.561	2.11	2135	860	2.568
	Water sand	9.049	2.483	2.21	2590	1060	2.326
Model 4	Shale	10.544	6.141	2.34	3240	1620	2.283
	Gas sand	0.874	2.459	2.07	1650	1090	1.936

reservoir fluid. Next, we will study how to construct a simultaneous inversion method for the dynamic DVRS and fluid factor to further improve the inversion accuracy and fluid identification ability of Russell fluid factor.

2.2. Prestack multi-parameter AVA nonlinear inversion

The LM method and the BDI method are the most commonly used methods for solving prestack multi-parameter AVA nonlinear inversion problems. The LM method does not need to provide well constraints. It has a low demand for logging curves. Theoretically, it is applicable even in areas where there are no or few well logging curves. However, with the change or increase of target inversion parameters, it is easy to fall into local minima, which leads to inaccurate inversion results. The BDI method can further reduce the multiplicity of inversion problems and improve the accuracy of inversion results by introducing a prior information contained in logging data. However, due to the limitations of logging technology or cost, it is difficult to obtain the logging curves of unconventional logging parameters in advance, which may limit the application of the BDI method. In this paper, we compare and analyze the capability and accuracy of the above two methods based on the simultaneous inversion problem of four parameters including the fluid factor, shear modulus, density and DVRS.

2.2.1. Iteratively regularizing Levenberg-Marquardt (IRLM) method

Based on the convolution model, the prestack seismic forward equation can be expressed as follows:

$$\mathbf{d} = \mathbf{G}(\mathbf{m}) + \mathbf{n}, \tag{3}$$

where, $\mathbf{d}$ represents the observed seismic data, $\mathbf{G}(\mathbf{m})$ represents the nonlinear forward operator based on Eq. (2), $\mathbf{m} = \begin{bmatrix} \mathbf{f} & \mu & \rho & \gamma^2_{dry} \end{bmatrix}$ represents the target parameter vector, and $\mathbf{n}$ represents the random noise.

Based on the forward equation shown in Eq. (3), the following objective functions can be constructed using the least squares principle:

$$L(\mathbf{m}) = \|(\mathbf{d} - \mathbf{G}(\mathbf{m}))\|^2 = (\mathbf{d} - \mathbf{G}(\mathbf{m}))^{\mathrm{T}}(\mathbf{d} - \mathbf{G}(\mathbf{m})). \tag{4}$$

Using a Taylor series expansion on the forward operator $\mathbf{G}(\mathbf{m})$ at the initial model parameters $\mathbf{m}^0$, we have:

$$\mathbf{G}(\mathbf{m}) = \mathbf{G}\left(\mathbf{m}^0\right) + \frac{\partial \mathbf{G}(\mathbf{m}^0)}{\partial \mathbf{m}}\Delta\mathbf{m} + \cdots. \tag{5}$$

Taking the first order approximation of Eq. (5) and substituting it into Eq. (4). Then, the solution expression of target parameter perturbation term based on the LM method can be given as follows:

$$\Delta\mathbf{m}^k = \left(\left(\frac{\partial \mathbf{G}\left(\mathbf{m}^k\right)}{\partial \mathbf{m}}\right)^{\mathrm{T}}\left(\frac{\partial \mathbf{G}\left(\mathbf{m}^k\right)}{\partial \mathbf{m}}\right) + \beta\mathbf{I}\right)^{-1}\left(\left(\frac{\partial \mathbf{G}\left(\mathbf{m}^k\right)}{\partial \mathbf{m}}\right) \times \left(\mathbf{d} - \mathbf{G}\left(\mathbf{m}^k\right)\right)\right), \tag{6}$$

where β is a Lagrange multiplier and $\mathbf{I}$ is an identity matrix.

Zhi et al. (2016) pointed out that the iteratively regularizing Levenberg-Marquardt (IRLM) method can minimizes the misfit between the observation data and model data at the same time by incorporating the Tikhonov regularization method, thereby improving the stability of the inversion algorithm. In this way, the solution expression shown in Eq. (6) can be rewritten as follows:

$$\Delta\mathbf{m}^k = \left(\left(\frac{\partial \mathbf{G}\left(\mathbf{m}^k\right)}{\partial \mathbf{m}}\right)^{\mathrm{T}}\left(\frac{\partial \mathbf{G}\left(\mathbf{m}^k\right)}{\partial \mathbf{m}}\right) + \beta_k\mathbf{I} + \beta_k\mathbf{D}^{\mathrm{T}}\mathbf{D}\right)^{-1}\left(\left(\frac{\partial \mathbf{G}\left(\mathbf{m}^k\right)}{\partial \mathbf{m}}\right)^{\mathrm{T}}\left(\mathbf{d} - \mathbf{G}\left(\mathbf{m}^k\right)\right) - \beta_k\mathbf{D}^{\mathrm{T}}\mathbf{D}\mathbf{m}^k\right), \tag{7}$$

where $\mathbf{D}$ is the first derivative operator, and the formula for parameter β_k is shown below:

$$\beta_k = \left\|\left(\mathbf{d} - \mathbf{G}\left(\mathbf{m}^k\right)\right)\right\|^2. \tag{8}$$

Based on Eq. (7), the updated iteration equation of the target parameters is given below:

$$\mathbf{m}^{k+1} = \mathbf{m}^k + \lambda^k\Delta\mathbf{m}^k, \quad k = 0,\ 1,\ 2.... \tag{9}$$

For iteration step size λ^k, Zhi et al. (2016) gave the strong Wolfe line search algorithm to obtain this parameter, which only needs to meet the following conditions:

$$L\left(\mathbf{m}^k + \lambda^k\Delta\mathbf{m}^k\right) \le L\left(\mathbf{m}^k\right) + \delta\lambda^k\left(\left(\frac{\partial \mathbf{G}\left(\mathbf{m}^k\right)}{\partial \mathbf{m}}\right)^{\mathrm{T}}\left(\mathbf{G}\left(\mathbf{m}^k\right) - \mathbf{d}\right), \Delta\mathbf{m}^k\right), \tag{10}$$

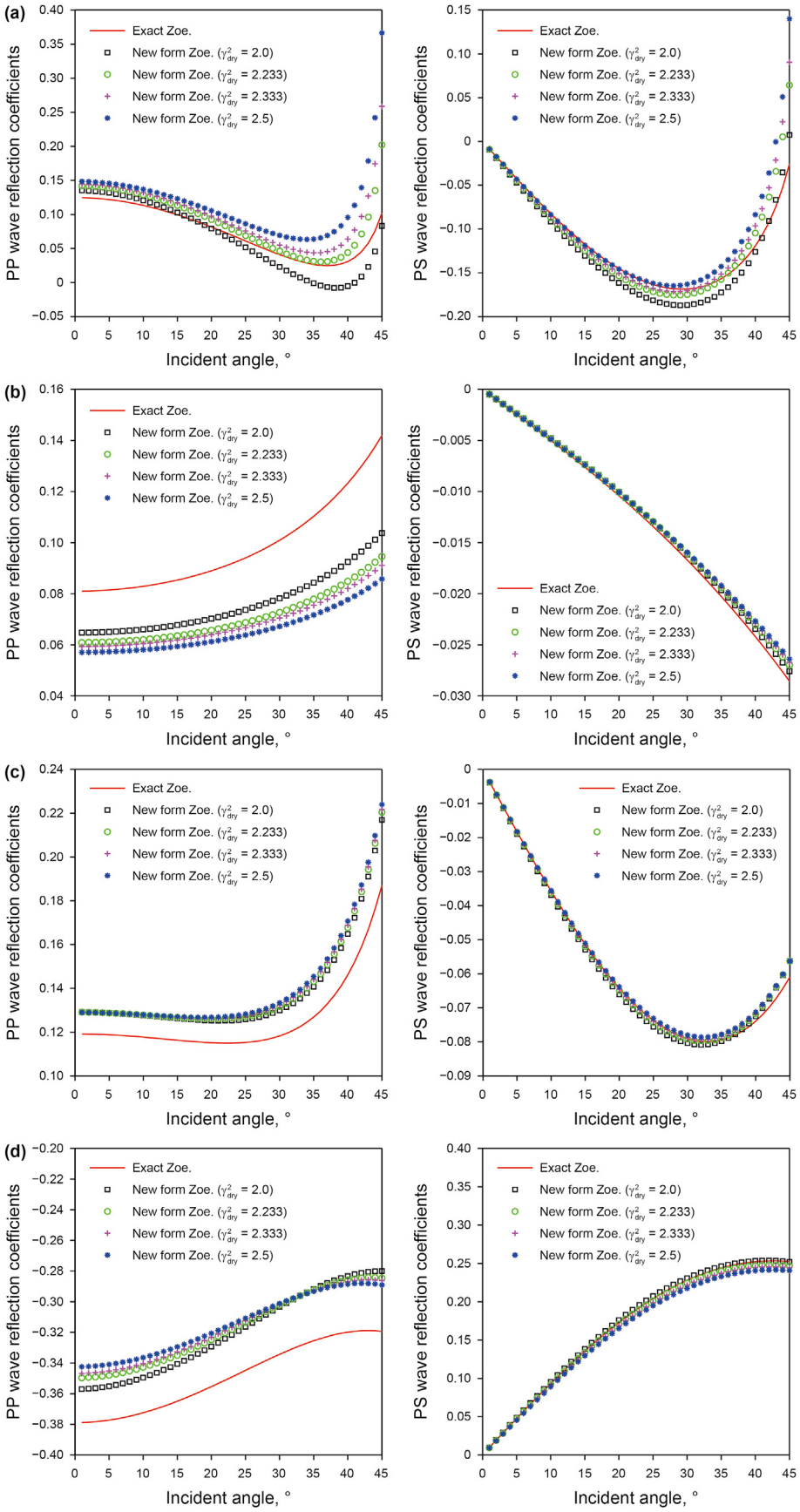

Fig. 1. Comparison of the exact Zoeppritz equations (red line) and the FMR-Zoeppritz equations with the different static γ^2_{dry} for four Models. (a) Model 1, (b) Model 2, (c) Model 3, (d) Model 4.

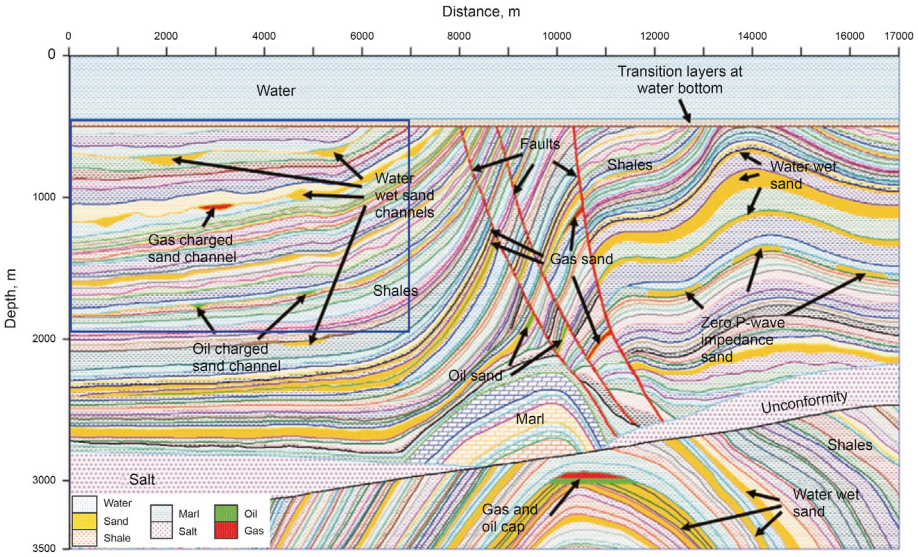

Fig. 2. Marmousi 2 model, the blue rectangle indicates the test area.

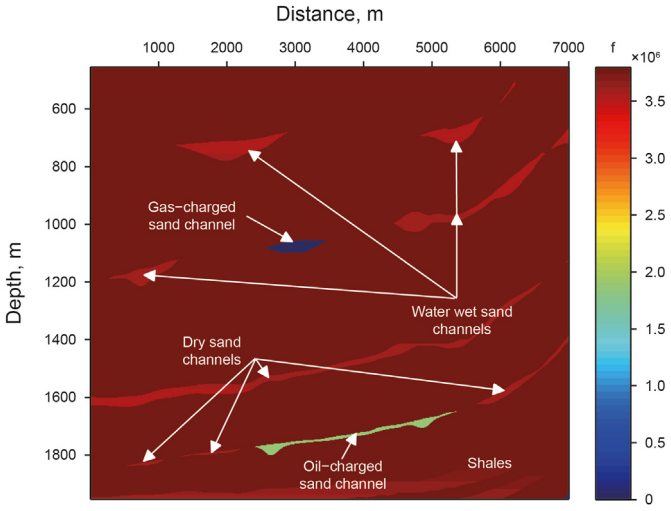

Fig. 3. The fluid factor f calculated by the static $\gamma^2_{\text{dry}} = 3.95$.

$$\left|\left(\Delta\mathbf{m}^k\right)^{\mathrm{T}}\left(\frac{\partial\mathbf{G}\left(\mathbf{m}^k+\lambda^k\Delta\mathbf{m}^k\right)}{\partial\mathbf{m}}\right)^{\mathrm{T}}\left(\mathbf{G}\left(\mathbf{m}^k+\lambda^k\Delta\mathbf{m}^k\right)-\mathbf{d}\right)\right| \leq -b\lambda^k\left(\Delta\mathbf{m}^k\right)^{\mathrm{T}}\left(\frac{\partial\mathbf{G}\left(\mathbf{m}^k\right)}{\partial\mathbf{m}}\right)^{\mathrm{T}}\left(\mathbf{G}\left(\mathbf{m}^k\right)-\mathbf{d}\right). \tag{11}$$

2.2.2. Bayesian deterministic inversion (BDI) method

According to the research of Zhou et al. (2021a), the expression of BDI objective function with differentiable Laplace distribution blockiness constraint term for four parameters simultaneous inversion is given below:

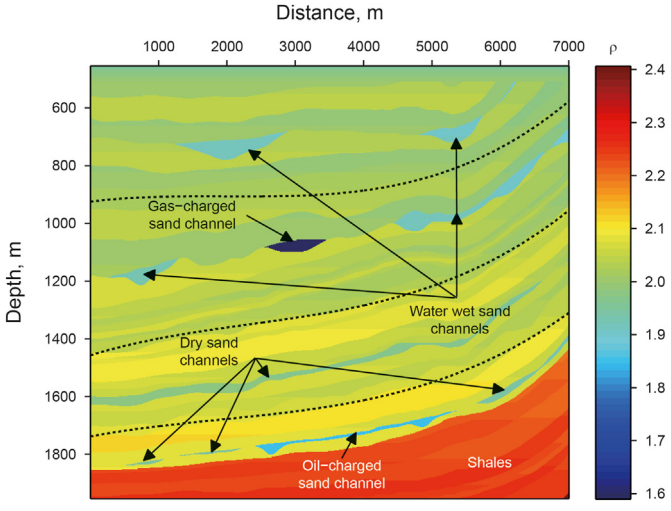

Fig. 4. The density in the extracted portion of the Marmousi 2 model.

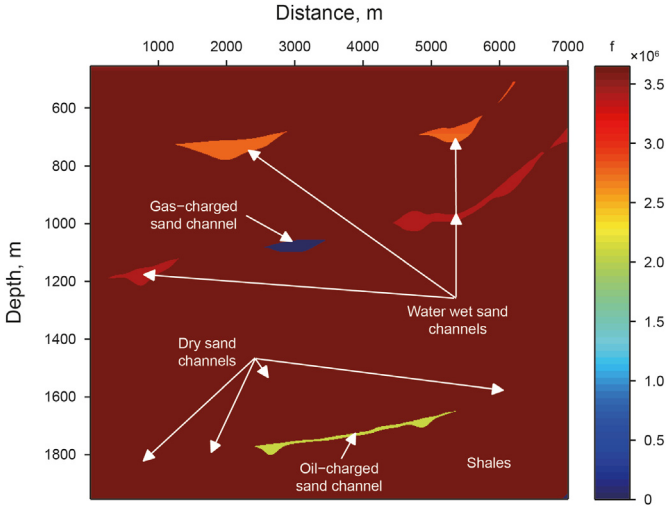

Fig. 5. The fluid factor f calculated by the dynamic γ^2_{dry}.

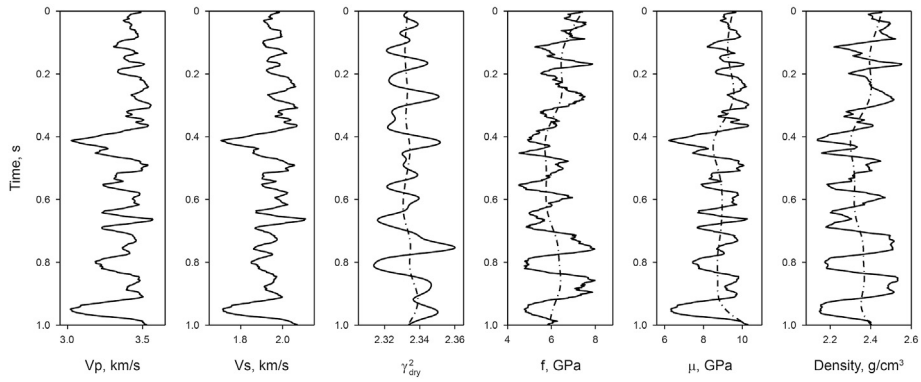

Fig. 6. The single-well model. The solid line represents true model data and the dashed line represents initial model data.

$$J(\mathbf{m}) = \frac{1}{2}(\mathbf{d}-\mathbf{G}(\mathbf{m}))^{\mathrm{T}}(\mathbf{d}-\mathbf{G}(\mathbf{m})) + \beta\left(\frac{1}{2}(\mathbf{m}-\mu)^{\mathrm{T}}\mathbf{C}_{\mathbf{m}}^{-1}(\mathbf{m}-\mu) + \sum_{l=1}^{4}\left(\sqrt{1+\frac{[\mathbf{D}(\mathbf{m}-\mu)]_l^2}{k_l^2}}-1\right)\right), \tag{12}$$

where, $\mathbf{C_m}$ is a covariance matrix containing the statistical correlations among four target parameters, which can be obtained from logging data, μ is the mean vector of target parameters, $\mathbf{D}$ is a first-order differential matrix, k_l, $l = 1, 2, 3, 4$ are scaling parameters (different for each target parameter) and $\beta = \sigma_n^2$ controls the weight of the prior information, where $\sigma_n{}^2$ represents the noise variance.

Taking the first order approximation of Eq. (5) and substituting it into Eq. (12). Then, we can obtain the solution expression of target parameter perturbation term based on the BDI method as follows:

$$\Delta\mathbf{m}^j = \left(\mathbf{H}\left(\mathbf{m}^j\right)\right)^{-1}\gamma\left(\mathbf{m}^j\right) = \left(\left(\frac{\partial\mathbf{G}(\mathbf{m}^j)}{\partial\mathbf{m}}\right)^{\mathrm{T}}\left(\frac{\partial\mathbf{G}(\mathbf{m}^j)}{\partial\mathbf{m}}\right) + \beta\left(\mathbf{C}_{\mathbf{m}}^{-1}+\mathbf{D}^{\mathrm{T}}\frac{1}{\sqrt{k_l^4+k_l^2[\mathbf{D}(\mathbf{m}^j-\mu)]_l^2}}\mathbf{D}\right)\right)^{-1} \times\left(\left(\frac{\partial\mathbf{G}(\mathbf{m}^j)}{\partial\mathbf{m}}\right)^{\mathrm{T}}\left(\mathbf{d}-\mathbf{G}\left(\mathbf{m}^j\right)\right) - \beta\left(\mathbf{C}_{\mathbf{m}}^{-1}+\mathbf{D}^{\mathrm{T}}\frac{1}{\sqrt{k_l^4+k_l^2[\mathbf{D}(\mathbf{m}^j-\mu)]_l^2}}\mathbf{D}\right)\left(\mathbf{m}^j-\mu\right)\right). \tag{13}$$

Based on the solution expression shown in Eq. (13), the target parameters can be updated iteratively:

$$\mathbf{m}^{j+1} = \mathbf{m}^j + \lambda^j\Delta\mathbf{m}^j,\ j = 0,\ 1,\ 2\ldots \tag{14}$$

where λ^j is step length of jth iteration. Similarly, this parameter can also be linearly searched using the constraints shown in Eqs. (10) and (11).

From the above formula derivation processes, we see that the essential difference between the LM method and BDI method is whether to introduce logging information to regularize the

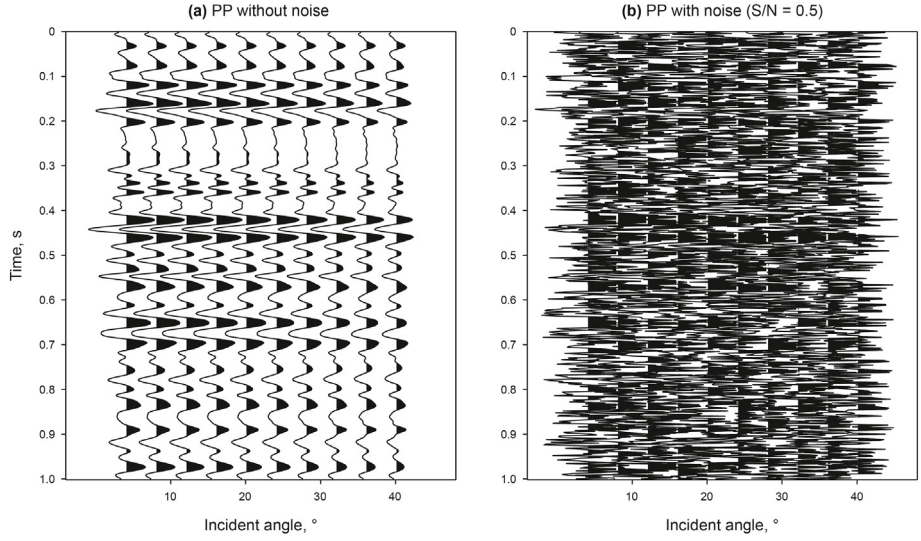

Fig. 7. Synthetic prestack angle gathers. (a) PP wave angle gathers without noise, (b) PP wave angle gathers with noise (S/N = 0.5).

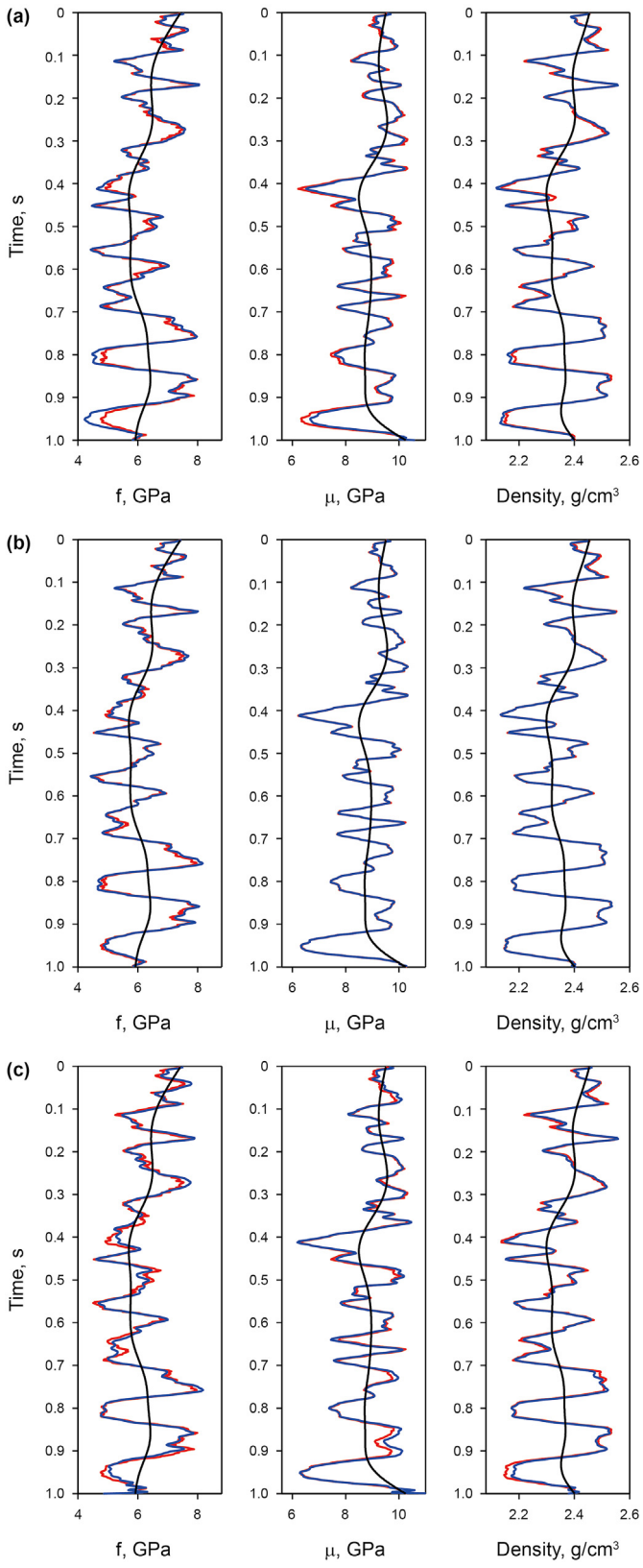

Fig. 8. PP wave inversion results by using the noise-free data (Inversion method proposed by Zhou et al. (2021a)). The black line indicates initial model data, blue line indicates inversion result and red line indicates true model data. (a) $\gamma^2_{dry} = 2.133$, (b) $\gamma^2_{dry} = 2.333$, and (c) $\gamma^2_{dry} = 2.533$.

inversion algorithm. Next, we will use synthetic data to compare the applicability of these two methods.

3. Synthetic data example

To facilitate comparison and highlight the advantages of the new method, we still use the single-well model shown in Fig. 6 given by Zhou et al. (2021a) for test analysis. Fig. 7a shows the synthetic PP wave angle gathers obtained by forward modeling of well curves shown in Fig. 6, where the sampling interval is 2 ms, and the seismic wavelet is the Ricker wavelet with the dominant frequency of 30 Hz.

Firstly, to demonstrate the influence of the static DVRS on the fluid factor inversion results, we use Eq. (1) to implement simultaneous inversion of three parameters based on a static DVRS value. Fig. 8a–c shows the corresponding inversion results when the static DVRS equals 2.133, 2.333 and 2.533, respectively. From Fig. 8, we see that changing the value of static DVRS has an obvious impact on the accuracy of the fluid factor inversion results. Even though its value is very close to the mean value of the dynamic DVRS parameter curve, the fluid factor inversion results still have obvious deviations in some places. In fact, the value of static DVRS is challenging to estimate accurately, limiting the estimation accuracy of existing method for the fluid factor. Therefore, to reduce the negative influence of static DVRS, it is necessary to take the parameter DVRS as a dynamic variable and simultaneously as a target inversion parameter.

Next, we use the single-well model shown in Fig. 6 to compare and analyze whether the IRLM method and the BDI method can successfully solve the four parameters simultaneous inversion problem proposed in this paper. Using the noise-free synthetic PP wave angle gathers shown in Fig. 7a, we implemented prestack inversion based on the IRLM method and the BDI method respectively. Fig. 9 shows the inversion results of the IRLM method. Fig. 10 shows the comparison between the PP wave angle gathers (input data) shown in Fig. 7a and the forward synthetic gather based on the inversion results (blue line) shown in Fig. 9 (synthetic data). From Figs. 9 and 10, the IRLM method is prone to fall into local minima when solving the four parameters simultaneous inversion problem, failing to accurately obtain the key parameter fluid factor. Fig. 11 shows the inversion results of the BDI method. It can be seen from the comparison between Figs. 8 and 11 that taking the DVRS as dynamic variable and simultaneously as target inversion parameter can further improve the inversion accuracy of the fluid factor, which verifies the feasibility and effectiveness of the new method.

To test the stability and anti-noise performance of the proposed method, the noisy PP wave data shown in Fig. 7b is obtained by adding random noise with a signal-to-noise ratio (S/N) of 0.5 to the synthetic data shown in Fig. 7a. The corresponding inversion results are shown in Fig. 12. We see that the four parameters simultaneous inversion algorithm based on the BDI method (proposed method) has good stability and anti-noise performance.

In addition, we also find that although the inversion accuracy of the parameter DVRS is significantly lower than the other three target parameters, this does not affect the estimation accuracy of the main target parameter fluid factor. The main reason for the relatively low estimation accuracy of parameter DVRS is that the true model data of DVRS given in our single-well model is relatively smoother than the other three parameters, which is a minor defect in our model design. The main purpose of our paper is to further improve the estimation accuracy of the Russell fluid factor. From the comparison of inversion results, we have achieved this goal. Moreover, the application of the parameter DVRS is not discussed in

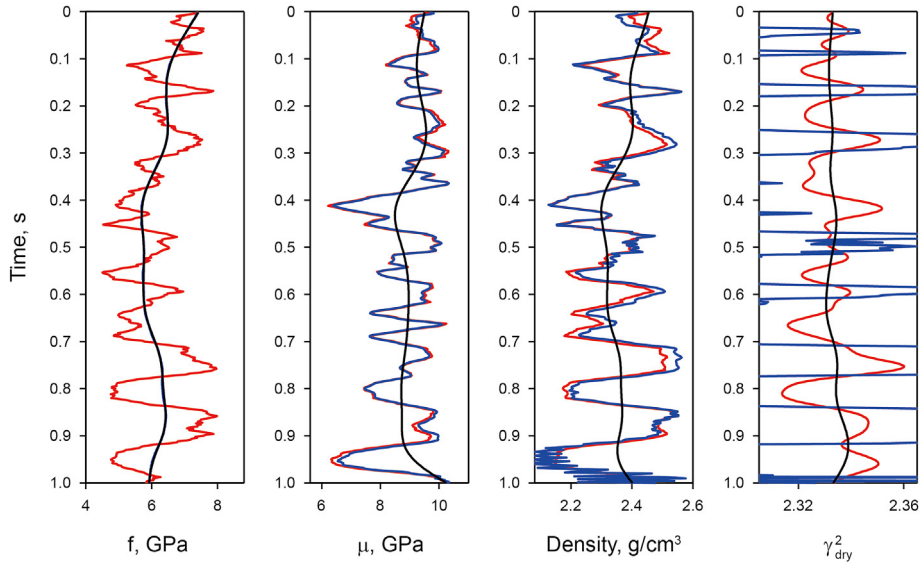

Fig. 9. PP wave inversion results by using the noise-free data (IRLM method). The black line indicates initial model data, blue line indicates inversion result and red line indicates true model data.

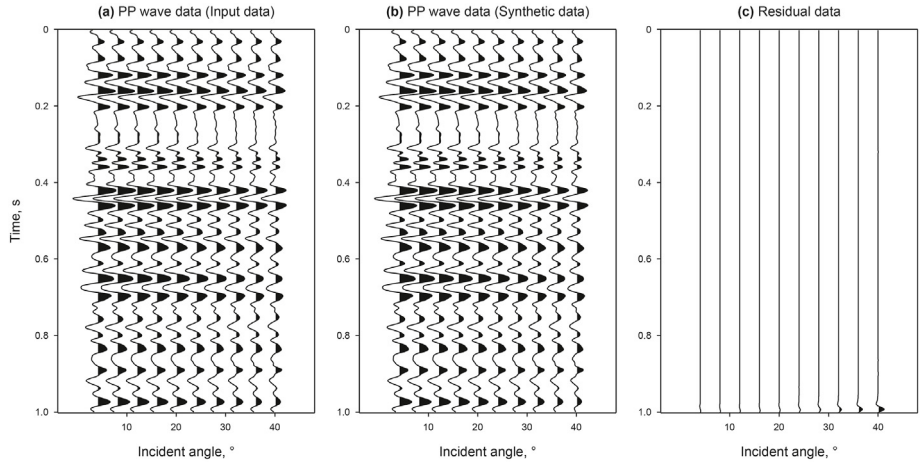

Fig. 10. Comparison between input gathers and synthetic gathers: (a) input data, (b) synthetic data and (c) residual data.

this paper, so the inversion results of the parameters DVRS will not be displayed and analyzed in subsequent inversion.

4. Field data example

The filed data used by Zhou et al. (2021a) is chosen in this paper to demonstrate the effectiveness and advantages of the new method. The test 2D PP wave angle gathers are extracted from a field located in Eastern China with an effective angle range of 3°–45°. The stacked section of test data is shown in Fig. 13. The locations of three known oil-bearing sandstone layers and two wells (Well A and Well B) are clearly indicated. Similarly, only Well A is used in the inversion and Well B is treated as a "blind" verification well. Fig. 14 shows the inversion result of the fluid factor obtained by the three parameters simultaneous inversion method based on a static DVRS value provided by Zhou et al. (2021a). Although the three oil sand layers can be finely identified and depicted, the oil-bearing reservoir and the non-reservoir in the middle are not effectively distinguished. This shows that the static DVRS, without considering the influence of lithology, depth and other factors, greatly limit the actual reservoir fluid identification quality of fluid factor inversion method based on the exact Zoeppritz equations. To solve this problem, we consider the impact of lithology and depth (or travel time) on the parameter DVRS and estimate a group of dynamic DVRS to reduce the adverse impact of the static DVRS on the identification ability and estimation accuracy of the fluid factor. Poisson's ratio and density have obvious advantages in lithology identification. Therefore, based on the Poisson's ratio and density logging curve shown in Fig. 15, we divide the test profile into four large layers in vertical direction, and then use the static value estimation method to estimate the DVRS values of corresponding large layers, which are 2.47, 2.43, 2.47 and 2.33 respectively. The black curve shown in Fig. 16 is the Russell fluid factor curve calculated using this group of dynamic DVRS values. In Fig. 17, we also give the comparison and the crossplot between the Russell fluid factor shown in Fig. 16 and oil saturation logging curve. It can be seen that the fluid factor curve calculated by the proposed method effectively identifies the oil-bearing sandstone reservoir and suppresses the illusions in the non-reservoir area. Based on this group of dynamic DVRS values and the calculated fluid factor curve,

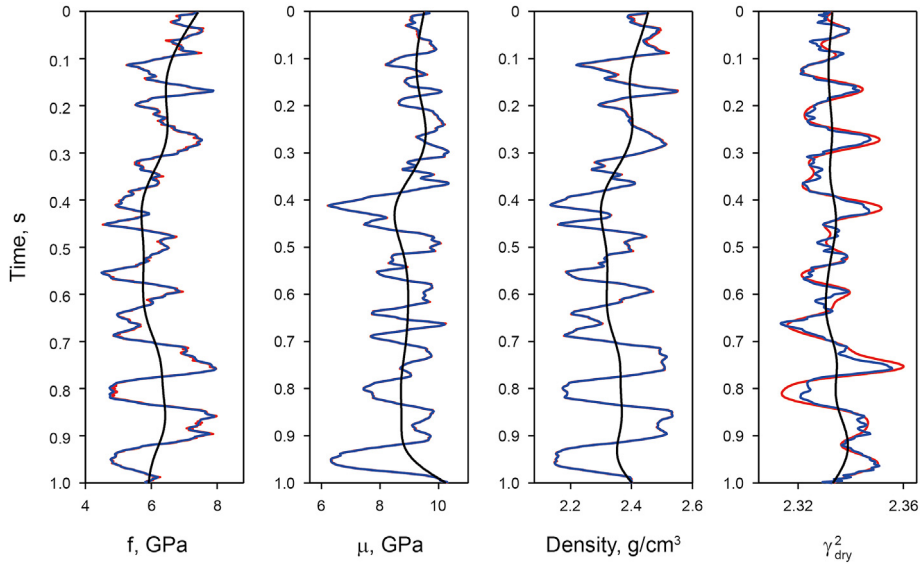

Fig. 11. PP wave inversion results by using the noise-free data (Proposed method). The black line indicates initial model data, blue line indicates inversion result and red line indicates true model data.

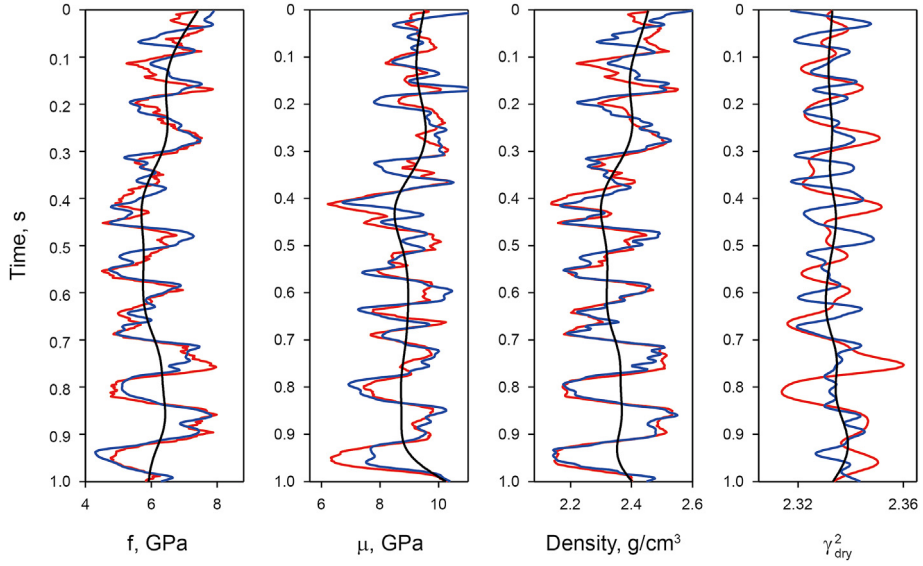

Fig. 12. PP wave inversion results with S/N = 0.5 (Proposed method). The black line indicates initial model data, blue line indicates inversion result and red line indicates true model data.

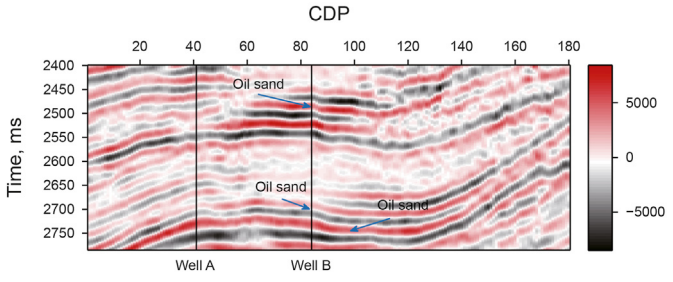

Fig. 13. 2D Poststack seismic data section. The black lines indicate the location of Well A and Well B.

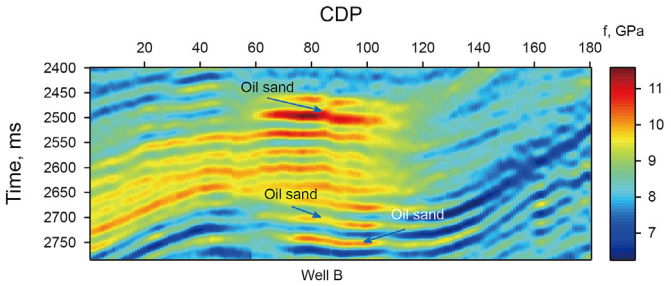

Fig. 14. Inversion results fluid factor (Zhou et al., 2021a).

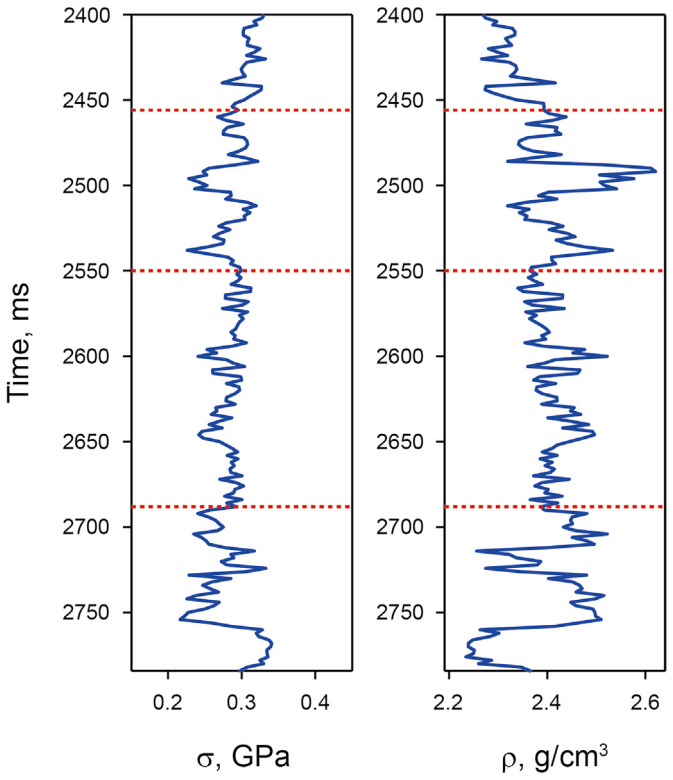

Fig. 15. Logging curves of Poisson's ratio and density. The red dotted line is the demarcation line of the large layer we defined.

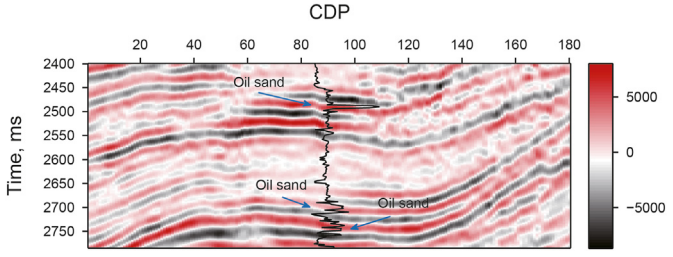

Fig. 16. 2D Poststack seismic data section. The black curve is the Russell fluid factor curve calculated using the dynamic DVRS.

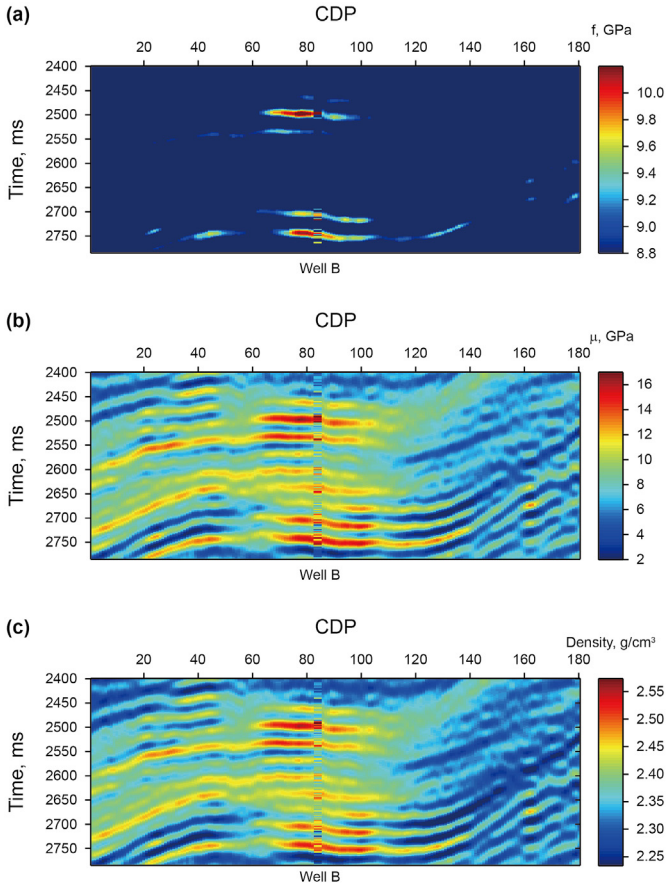

Fig. 18. Inversion results section of the proposed method: (a) fluid factor, (b) shear modulus, (c) density.

we carried out the inversion test based on the proposed method. Fig. 18 shows the inversion profiles of the fluid factor, shear modulus and density. To clearly depict the oil bearing reservoirs using the fluid factor inversion results, we set the values represented by the color bar in Fig. 18a based on the analysis results in Fig. 17. Fig. 19 shows the inversion results at the location of Well B. The comparison between Figs. 14 and 18a demonstrates that the fluid factor estimated by the proposed method can finely depict the

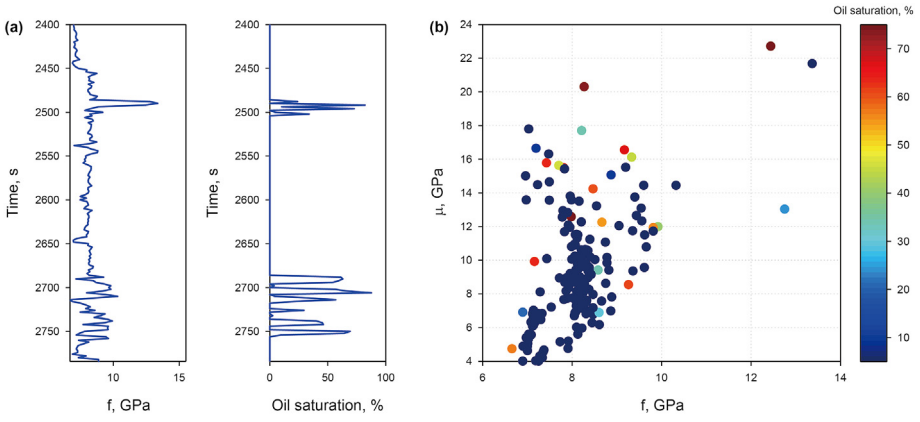

Fig. 17. The comparison and the crossplot between the Russell fluid factor shown in Fig. 16 and oil saturation logging curve.

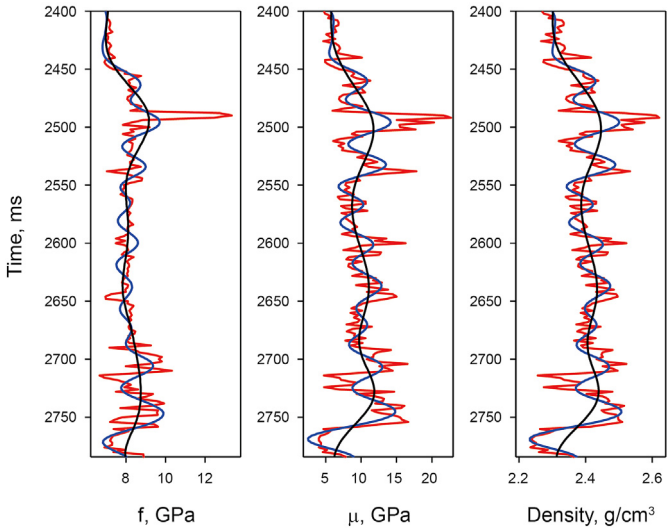

Fig. 19. Inversion results of proposed method at the Well B location. The red lines indicates the well curves, the blue lines indicates the inversion results and the black lines indicates the initial model.

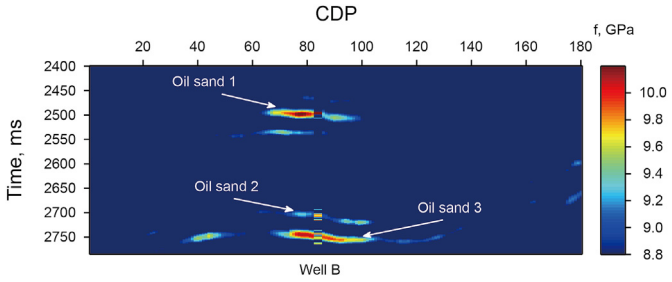

Fig. 20. Inversion results fluid factor (the static DVRS).

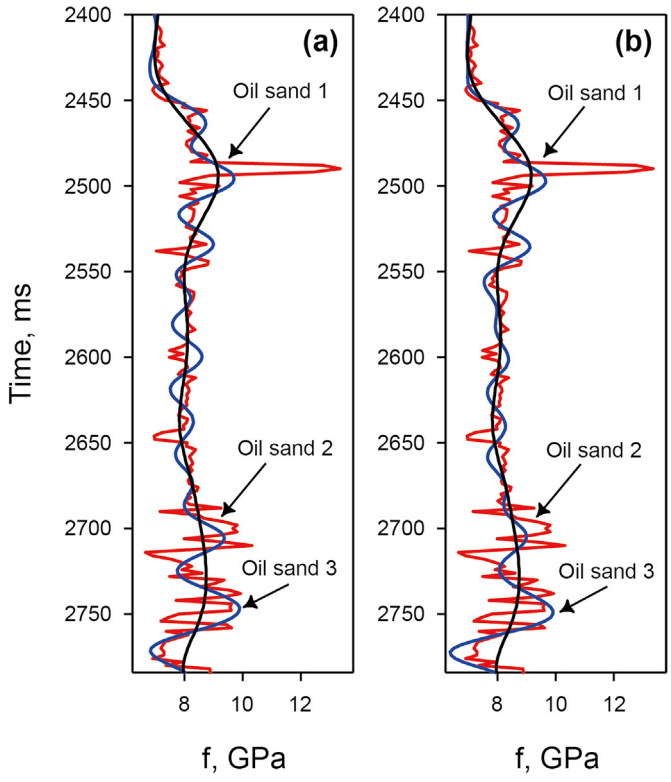

Fig. 21. Comparison of fluid factor inversion results at the Well B location. The red lines indicates the well curves, the blue lines indicates the inversion results and the black lines indicates the initial model: (a) proposed method, and (b) conventional method proposed by Zhou et al. (2021a).

oil-bearing sandstone reservoir and suppress the illusions in other non-reservoir areas.

In addition, to further demonstrate the influence of the static DVRS on the accuracy of the fluid factor inversion result, we use Russell fluid factor curve shown in Fig. 16 to perform the three parameters simultaneous inversion based on a static DVRS. The corresponding fluid factor inversion results are shown in Figs. 20 and 21b. From the comparison between Figs. 19a and Fig. 20, and the comparison between Fig. 21a and b, the proposed method can further improve the characterizing accuracy of oil sand layer 2. In conclusion, the proposed method can effectively overcome the adverse influence of the static DVRS on Russell fluid factor fluid identification ability and estimation accuracy, and further improve the applicability of fluid factor inversion methods based on the exact Zoeppritz equations, which demonstrates the advantages of our method.

5. Discussion

In this paper, we propose a new method to further improve the Russell fluid factor fluid detection ability and estimation accuracy using the dynamic DVRS. Through theoretical analysis and comparison of synthetic data, it can be seen that compared with the IRLM method without well constraint, the BDI method based on the prior information constraint of logging data is more suitable for solving the four parameters simultaneous inversion problem, which means that it is essential to estimate the dynamic DVRS curve varying with depth and lithology in advance. The field data test shows that in the area with simple lithological changes, using large-scale means to approximately estimate a group of simple dynamic DVRS values in blocks can also improve the fluid discrimination ability and estimation accuracy of the Russell fluid factor. However, for complicated reservoirs, if we continue to use large-scale means to estimate the dynamic DVRS curve at the well location in advance and then apply it to Russell fluid factor calculation and inversion, it will reduce the identification ability and estimation accuracy of the fluid factor. This is the limitation of the new method. Therefore, how to estimate the dynamic DVRS curve changing with depth and lithology needs to be further studied. In further work, we will solve the problem of fluid identification for complicated reservoirs and improve the quality of fluid discrimination.

6. Conclusions

The analysis results based on a portion of the Marmousi 2 model, numerical forward modeling and synthetic data inversion test show that the static DVRS will seriously degrade the fluid identification ability and estimation accuracy of the fluid factor. To reduce the adverse effects of the static DVRS, we propose a four parameters simultaneous inversion method for the Russell fluid factor by treating the DVRS as a dynamic variable for the first time. From the analysis of the extracted portion of the Marmousi 2 model, we find that the selection of dynamic DVRS varying with lithology and depth can significantly improve the fluid identification quality of the fluid factor. Synthetic data example shows that the BDI method is more suitable than the IRLM method to solve the four-parameter simultaneous inversion problem proposed in our

paper, and the new method can further improve the estimation accuracy of the Russell fluid factor. The field data application example demonstrates that the proposed method cannot only clearly depict the fluid-bearing reservoir, but also effectively distinguish the fluid-bearing reservoir from the non-reservoir, and further improve the accuracy of the fluid factor inversion result, which comprehensively verifies the feasibility and effectiveness of the proposed method.

From the discussion part, it is essential to develop a high-accuracy pseudo-well logging curve construction method for the DVRS parameter, which is one of the important research directions in the future. In addition, combining the dynamic DVRS with the effective pore-fluid bulk modulus to improve the quality of reservoir fluid identification is also worthy of further research.

Declaration of competing interest

The authors declare that they have no known competing financial interests or personal relationships that could have appeared to influence the work reported in this paper.

Acknowledgments

We would like to express our gratitude to the sponsorship of the National Natural Science Foundation of China (41904116, 41874156, 42074167 and 42204135), the Natural Science Foundation of Hunan Province (2020JJ5168) and the China Postdoctoral Science Foundation (2021M703629) for their funding of this research.

References

Ali, M., Ma, H.L., Pan, H.P., Ashraf, U., Jiang, R., 2020. Building a rock physics model for the formation evaluation of the Lower Goru sand reservoir of the Southern Indus Basin in Pakistan. J. Pet. Sci. Eng. 194, 107461. https://doi.org/10.1016/j.petrol.2020.107461.

Ashraf, U., Zhang, H.C., Anees, A., Ali, M., Zhang, X.N., Abbasi, S.S., Mangi, H.N., 2020. Controls on reservoir heterogeneity of a shallow-marine reservoir in Sawan Gas Field, SE Pakistan: implications for reservoir quality prediction using acoustic impedance inversion. Water 12 (11), 2972. https://doi.org/10.3390/w12112972.

Ashraf, U., Zhang, H.C., Anees, A., Mangi, H.N., Ali, M., Zhang, X.N., Imraz, M., Abbasi, S.S., Abbas, A., Ullah, Z., Tan, S.C., 2021. A core logging, machine learning and geostatistical modeling interactive approach for subsurface imaging of lenticular geobodies in a clastic depositional system, SE Pakistan. Nat. Resour. Res. 30, 2807–2830. https://doi.org/10.1007/s11053-021-09849-x.

Bing, P.P., Cao, S.Y., Lu, J.T., 2012. Non-linear AVO inversion based on support vector machine. Chinese J. Geophys-CH. 2012 55 (3), 1025–1032. https://doi.org/10.6038/j.issn.0001-5733.2012.03.033 (in Chinese).

Chen, G., Wang, X.J., Wu, B.C., Qi, H.Y., Xia, M.M., 2018. Computation of dry-rock VP/VS ratio, fluid property factor, and density estimation from amplitude-variation-with-offset inversion. Geophysics 83 (6), R669–R679. https://doi.org/10.1190/geo2017-0621.1.

Du, Q.Z., Yan, H.Z., 2013. PP and PS joint AVO inversion and fluid prediction. J. Appl. Geophys. 90, 110–118. https://doi.org/10.1016/j.jappgeo.2013.01.005.

Du, B.Y., Yang, W.Y., Zhang, J., Yong, X.S., Gao, J.H., Li, H.S., 2019. Matrix-fluid decoupling-based joint PP-PS-wave seismic inversion for fluid identification. Geophysics 84 (3), R477–R487. https://doi.org/10.1190/geo2017-0376.1.

Goodway, W.N., Chen, T., Downton, J., 1997. Improved AVO fluid detection and lithology discrimination using Lamé petrophysical parameters; "λρ," "μρ" and "λ/μ fluid stack," from P and S inversions. In: 67th Annual International Meeting, SEG, Expanded Abstracts, pp. 183–186. https://doi.org/10.1190/1.1885795.

Gray, F., Chen, T., Goodway, W., 1999. Bridging the gap: using AVO to detect changes in fundamental elastic constants. In: 69th Annual International Meeting, SEG, Expanded Abstracts, pp. 852–855. https://doi.org/10.1190/1.1821163.

Huang, W.L., Gao, F., Liao, J.P., Chuai, X.Y., 2020. A deep learning network for estimation of seismic local slopes. Pet. Sci. 18 (6), 92–105. https://doi.org/10.1007/s12182-020-00530-1.

Levenberg, K., 1944. A method for the solution of certain non-linear problems in least squares. Q. Appl. Math. 2, 164–168. https://www.jstor.org/stable/43633451.

Li, C.N., 2014. Multi-wave Joint AVA Attributes Extraction and Hydrocarbon Prediction. Master's Thesis. China University of Petroleum, Qingdao.

Lu, J., Yang, Z., Wang, Y., Shi, Y., 2015. Joint PP and PS AVA seismic inversion using exact Zoeppritz equations. Geophysics 80 (5), R239–R250. https://doi.org/10.1190/geo2014-0490.1.

Lu, J., Wang, Y., Chen, J.Y., An, Y., 2018. Joint anisotropic amplitude variation with offset inversion of PP and PS seismic data. Geophysics 83 (2), N31–N50. https://doi.org/10.1190/geo2016-0516.1.

Liu, X.Y., Zhou, L., Chen, X.H., Li, J.Y., 2020. Lithofacies identification using support vector machine based on local deep multi-kernel learning. Pet. Sci. 17, 954–966. https://doi.org/10.1007/s12182-020-00474-6.

Liu, X.Y., Shao, G., Yuan, C., Chen, X.H., Li, J.Y., Chen, Y.K., 2022a. Mixture of relevance vector regression experts for reservoir properties prediction. J. Pet. Sci. Eng. 214, 110498. https://doi.org/10.1016/j.petrol.2022.110498.

Liu, X., Shao, G., Liu, Y., Liu, X., Li, J., Chen, X., Chen, Y., 2022b. Deep classified autoencoder for lithofacies identification. Trans. Geosci. Remote. Sens. 60, 5909914. https://doi.org/10.1109/TGRS.2021.3139931.

Marquardt, D.W., 1963. An algorithm for least-squares estimation of nonlinear inequalities. J. Soc. Ind. Appl. Math. 11, 431–441. https://www.jstor.org/stable/2098941.

Martin, G.S., Wiley, R., Martfurt, K.J., 2006. Marmousi2: an elastic upgrade for Marmousi. Lead. Edge 25, 156–166. https://doi.org/10.1190/1.2172306.

Nocedal, J., Wright, S.J., 2006. Numerical Optimization, second ed. Springer. https://doi.org/10.1007/0-387-22742-3_18.

Russell, B., Hedlin, K., Hilterman, F., Lines, L., 2003. Fluid-property discrimination with AVO: a Biot-Gassmann perspective. Geophysics 68, 29–39. https://doi.org/10.1190/1.1543192.

Russell, B., Gray, D., Hampson, D., 2011. Linearized AVO and poroelasticity. Geophysics 76 (3), C19–C29. https://doi.org/10.1190/1.3555082.

Smith, G.C., Gidlow, P.M., 1987. Weighted stacking for rock property estimation and detection of gas. Geophys. Prospect. 35 (9), 993–1014. https://doi.org/10.1111/j.1365-2478.1987.tb00856.x.

Wang, P., Li, J.Y., Chen, X.H., Wang, B.F., 2020. Joint probabilistic fluid discrimination of tight sandstone reservoirs based on Bayes discriminant and deterministic rock physics modeling. J. Pet. Sci. Eng. 191, 107218. https://doi.org/10.1016/j.petrol.2020.107218.

Wang, P., Chen, X.H., Li, X.Y., Cui, Y.A., Li, J.Y., Wang, B.F., 2021. Analysis and estimation of an inclusion-based effective fluid modulus for tight gas-bearing sandstone reservoirs. IEEE Trans. Geosci. Rem. Sens. 60, 1–10. https://doi.org/10.1109/TGRS.2021.3099134.

Yin, X.Y., Zhang, S.X., 2014. Bayesian inversion for effective pore-fluid bulk modulus based on fluid-matrix decoupled amplitude variation with offset approximation. Geophysics 79 (5), R221–R232. https://doi.org/10.1190/GEO2013-0372.1.

Zong, Z.Y., Yin, X.Y., Wu, G.C., 2013. Direct inversion for a fluid factor and its application in heterogeneous reservoirs. Geophys. Prospect. 61, 998–1005. https://doi.org/10.1111/1365-2478.12038.

Zhe, Y., Gu, H.M., 2013. Non-linear prestack seismic inversion with global optimization using an edge-preserving smoothing filter. Geophys. Prospect. 61, 747–760. https://doi.org/10.1111/1365-2478.12001.

Zhou, L., Chen, Z.C., Li, J.Y., Chen, X.H., Liu, X.Y., Liao, J.P., 2020. Nonlinear amplitude versus angle inversion for transversely isotropic media with vertical symmetry axis using new weak anisotropy approximation equations. Pet. Sci. 17 (3), 628–644. https://doi.org/10.1007/s12182-020-00445-x.

Zhou, L., Liu, X.Y., Li, J.Y., Liao, J.P., 2021a. Robust AVO inversion for the fluid factor and shear modulus. Geophysics 86 (4), R471–R483. https://doi.org/10.1190/GEO2020-0234.1.

Zhou, L., Liao, J.P., Li, J.Y., Chen, X.H., Liu, X.Y., 2021b. Prediction method of reservoir oil-gas potential based on exact Zoeppritz equations. Chinese J. Geophys-CH. 64 (10), 3788–3806. https://doi.org/10.6038/cjg2021P0099 (in Chinese).

Zhou, L., Li, J.Y., Yuan, C., Liao, J.P., Chen, X.H., Liu, Y.X., Pan, S.L., 2022. Bayesian deterministic inversion based on the exact reflection coefficients equations of transversely isotropic media with a vertical symmetry axis. Trans. Geosci. Remote Sens. 60, 1–15. https://doi.org/10.1109/TGRS.2022.3176628.

Zhi, L.X., Chen, S.Q., Li, X.Y., 2016. Amplitude variation with angle inversion using the exact Zoeppritz equations — theory and methodology. Geophysics 81 (2), N1–N15. https://doi.org/10.1190/geo2014-0582.1.